Journal of Solid State Chemistry 184 (2011) 21–29

Contents lists available at ScienceDirect

Journal of Solid State Chemistry

journal homepage: www.elsevier.com/locate/jssc

Ternary rare-earth bismuthides RE_5SiBi_2 and RE_5GeBi_2 (RE=La–Nd, Gd–Er): Stabilization of the β-Yb_5Sb_3-type structure through tetrel substitution

Stephen D. Barry, Andriy V. Tkachuk, Haiying Bie, Peter E.R. Blanchard, Arthur Mar*

Department of Chemistry, University of Alberta, Edmonton, Alberta, Canada T6G 2G2

ARTICLE INFO

Article history:
Received 21 June 2010
Received in revised form
22 September 2010
Accepted 3 October 2010
Available online 13 October 2010

Keywords:
Rare earths
Bismuthides
Crystal structure
XPS
Magnetic properties

ABSTRACT

Ternary bismuthides RE_5TtBi_2 containing rare-earth (RE=La–Nd, Gd–Er) and tetrel (Tt=Si, Ge) atoms have been prepared by arc-melting of the elements followed by annealing at 800 °C. They adopt the β-Yb_5Sb_3-type structure (Pearson symbol o$P32$, space group $Pnma$, Z=4), as revealed through analysis by single-crystal X-ray diffraction on $Ce_5Si_{0.869(4)}Bi_{2.131(4)}$ and powder X-ray diffraction on Ce_5GeBi_2. Cell parameters for the entire series lie in the ranges of a=12.8–11.8 Å, b=9.6–9.0 Å, and c=8.4–7.9 Å. Solid solubility in $Ce_5Si_xBi_{3-x}$ and $Pr_5Si_xBi_{3-x}$ (approximately $0.9 \le x \le 1.2$, depending on the RE member) is much more limited compared to the antimonides, consistent with a highly ordered structure in which the two possible anion sites are essentially segregated into a smaller one occupied by Tt atoms (CN7) and a larger one occupied by Bi atoms (CN9). Band structure calculations on La_5SiBi_2 confirm the importance of La–La bonding interactions near the Fermi level. X-ray photoelectron spectra support the presence of partially anionic Bi atoms, as indicated by a small negative binding energy shift relative to elemental Bi. The Ce and Pr members undergo magnetic transitions at low temperatures, possibly involving ferromagnetic interactions, that are strongly influenced by the nature of the Tt atom.

1. Introduction

Ternary rare-earth bismuthides are still sparse relative to the antimonides [1]. Among the few containing a triel (group 13) or tetrel (group 14) component, $LaGaBi_2$ [2] adopts a unique structure whereas $Eu_{14}InBi_{11}$ [3] and $CeGeBi_2$ [4] are isostructural to transition-metal analogues. $Gd_5Si_{4-x}Bi_x$ is a recently discovered series in which mixing of Si and Bi atoms leads to the development of new stacking polymorphs [5]. Previously we described the preparation of rare-earth tetrel antimonides $RE_5Tt_xSb_{3-x}$ (Tt=Si, Ge; usually $x \ge 1$) [6] that exhibit subtle differences in site preferences compared to the transition-metal counterparts $RE_5M_xSb_{3-x}$ (M=Fe, Co, Ni, Cu; $x \le 1$) [7–12]. This formulation emphasizes the disorder that takes place when Tt or M atoms partially substitute for Sb atoms in the β-Yb_5Sb_3-type structure adopted [13]; however, x does not extend to 0 or 3, i.e. the parent binaries have different structures. The idealized composition, if complete ordering takes place, is RE_5TtSb_2 or RE_5MSb_2. A few examples of the corresponding rare-earth transition-metal bismuthides RE_5MBi_2 (M=Fe, Co, Ni, Cu) have been sporadically reported, but definitive characterization is lacking [8,11,12]. Some of these compounds, such as $Gd_5Ni_{0.96}Sb_{2.04}$ and $Dy_5Ni_{0.66}Bi_{2.34}$, have begun to be investigated for their potential as magnetocaloric materials [11,12]. Given that the binary rare-earth bismuthides RE_5Bi_3 crystallize in other structure types (Mn_5Si_3- and Y_5Bi_3-type) [14–16], it is of interest to determine if incorporation of a Tt atom will also result in the formation of a β-Yb_5Sb_3-type structure.

We report here the preparation of the rare-earth tetrel bismuthides RE_5TtBi_2 (Tt=Si, Ge), seeking to elucidate how they differ from the other series in terms of the extent of RE substitution, solid solubility, and site preferences, with the aid of crystallographic analyses and band structure calculations. Magnetic studies were carried out on the Ce and Pr members of this series, and X-ray photoelectron spectra were measured for RE_5GeBi_2 (RE=La, Ce).

2. Experimental

2.1. Synthesis

Starting materials were RE pieces (Hefa, Aldrich, and Cerac), Si lumps (Alfa-Aesar), Ge ingots (Alfa), and Bi pieces (Cerac), each with 99.9% or better purity. Crystals of Ce_5SiBi_2 used for the structure determination were first identified in the course of investigating the Ce–Zn–Bi system [17,18], presumably as a byproduct obtained through deleterious reaction with the silica tube. Systematic reactions were subsequently carried out by arc-melting the elemental components in the stoichiometry "RE_5TtBi_2" (Tt=Si, Ge) on a scale of 0.3–0.5 g, with a 5–7 wt% excess of Bi added to compensate for its volatilization, in an Edmund Bühler MAM-1 compact arc melter on a water-cooled copper

* Corresponding author. Fax: +1 780 492 8231.
E-mail address: arthur.mar@ualberta.ca (A. Mar).

0022-4596/$ - see front matter © 2010 Elsevier Inc. All rights reserved.
doi:10.1016/j.jssc.2010.10.007

Table 1
Cell parameters for RE_5TtBi_2 (Tt=Si, Ge) phases.[a]

Compound[b]	a (Å)	b (Å)	c (Å)	V (Å^3)
$La_5Si_{1.0}Bi_{2.0}$	12.798(1)	9.567(1)	8.418(1)	1030.6(2)
$Ce_5Si_{0.9}Bi_{2.1}$	12.639(2)	9.509(2)	8.291(1)	996.4(2)
$Pr_5Si_{1.3}Bi_{1.7}$	12.528(1)	9.449(1)	8.248(1)	976.4(1)
$Nd_5Si_{1.2}Bi_{1.8}$	12.397(3)	9.344(2)	8.211(1)	951.2(3)
$Gd_5Si_{1.2}Bi_{1.8}$	12.076(3)	9.198(2)	8.049(1)	894.1(2)
$Tb_5Si_{1.2}Bi_{1.8}$	11.981(3)	9.126(2)	7.998(1)	874.5(2)
$Dy_5Si_{1.2}Bi_{1.8}$	11.898(2)	9.140(2)	7.984(1)	868.3(2)
$Ho_5Si_{1.2}Bi_{1.8}$	11.844(2)	9.023(2)	7.922(1)	846.6(2)
$Er_5Si_{1.1}Bi_{1.9}$	11.799(4)	9.035(3)	7.910(2)	843.3(3)
$La_5Ge_{1.2}Bi_{1.8}$	12.814(3)	9.604(3)	8.437(2)	1038.3(4)
$Ce_5Ge_{1.2}Bi_{1.8}$	12.589(3)	9.547(3)	8.304(2)	998.1(3)
$Pr_5Ge_{1.2}Bi_{1.8}$	12.445(2)	9.439(2)	8.236(2)	967.5(3)
$Nd_5Ge_{1.2}Bi_{1.8}$	12.401(5)	9.413(4)	8.228(2)	960.5(5)
$Gd_5Ge_{1.2}Bi_{1.8}$	12.051(3)	9.247(3)	8.065(2)	898.7(3)
$Tb_5Ge_{1.2}Bi_{1.8}$	11.974(3)	9.199(2)	8.029(1)	884.4(3)
$Dy_5Ge_{1.1}Bi_{1.9}$	11.902(3)	9.131(3)	7.978(2)	867.0(3)
$Ho_5Ge_{1.2}Bi_{1.8}$	11.862(3)	9.062(3)	7.959(2)	855.5(4)
$Er_5Ge_{1.1}Bi_{1.9}$	11.802(5)	9.034(4)	7.950(3)	847.6(3)

[a] Refined from powder X-ray diffraction data.
[b] Nominal composition determined on the basis that weight loss after arc-melting is attributed to volatilization of Bi.

hearth under an argon atmosphere gettered with Ti. The alloys were melted twice to ensure homogeneity, sealed within evacuated fused-silica tubes, and annealed at 800 °C for at least 2 weeks. No mass change (to within ± 0.1 mg) was observed after annealing, which excludes the possibility of contamination from the fused-silica container. Reactions for all *RE* from La to Lu (except Pm and Eu) were attempted. The desired ternary phases were obtained for *RE*=La–Nd and Gd–Er, as confirmed by powder X-ray diffraction patterns (Figs. S1 and S2 in Supplementary Data) collected on an Inel powder diffractometer equipped with a CPS 120 detector, but not for *RE*=Sm, Tm, Yb, and Lu. Within the detection limits of powder X-ray diffraction, most samples are either phase-pure or contained up to ~10% of other phases, typically RE_4Bi_3 or *RE*Bi, these impurities generally increasing with the later *RE* members; the Gd_5GeBi_2 and Er_5GeBi_2 samples suffered from significant impurities of binary phases. Table 1 lists the nominal compositions determined on the assumption that all weight loss occurring during the arc-melting originated from Bi volatilization, which was difficult to control. We estimate the uncertainty of these compositions to be within one decimal place (e.g., "$RE_5Tt_{1.0(1)}Bi_{2.0(1)}$"). As a measure of the reproducibility of these reactions, it can be noted that in a series of reactions "$Nd_5Si_xBi_{3-x}$", the desired ternary phase was obtained in 7 out of 10 reactions as the major or only product, whereas the unsuccessful reactions were associated with excessive Bi loss. These samples are moderately air-sensitive, their surfaces becoming visibly oxidized within hours or days. Selected samples were polished and embedded in resin for examination on a Zeiss EV MA15 scanning electron microscope. Semiquantitative energy-dispersive X-ray (EDX) analysis revealed average compositions (62–65% *RE*, 12–16% *Tt*, 22–25% Bi) close to expectations (62% *RE*, 13% *Tt*, 25% Bi) for the ideal composition RE_5TtBi_2 (Table S1 in Supplementary Data).

To determine the homogeneity range, reactions with starting compositions "$Ce_5Si_xBi_{3-x}$" ($0.8 \le x \le 1.1$) in increments of 0.1 and "$Pr_5Si_xBi_{3-x}$" ($0.5 \le x \le 1.6$) in increments of 0.2–0.3 were conducted with the same procedure as above. For $Ce_5Si_xBi_{3-x}$, inspection of the trend in cell parameters (Table S2 in Supplementary Data) suggests that the phase width is quite narrow, $0.9 \le x < 1.0$. For $Pr_5Si_xBi_{3-x}$, single-phase products were only obtained for $Pr_5Si_{1.0}Bi_{2.0}$, and $Pr_5Si_{1.2}Bi_{1.8}$, also establishing a narrow phase width of $0.9 \le x \le 1.2$. Phase widths for the other *RE* members were not determined, but are assumed to be similarly narrow.

2.2. Structure determination

Single-crystal X-ray diffraction data on the original Ce_5SiBi_2 crystal were collected on a Bruker Platform/SMART 1000 CCD diffractometer at 22 °C using ω scans. (Attempts were made to analyze numerous samples prepared from stoichiometric reactions, but these proved to be unsuccessful because of poor crystal quality.) Structure solution and refinement were carried out with use of the SHELXTL (version 6.12) program package [19]. Face-indexed numerical absorption corrections were applied. The centrosymmetric space group *Pnma* was chosen on the basis of intensity statistics. Initial atomic positions found by direct methods were consistent with the expected β-Yb_5Sb_3-type structure [13]. In accordance with the idealized model Ce_5SiBi_2, the two possible anion sites were occupied in an ordered fashion, with Bi atoms exclusively in the 8*d* site and Si atoms in the 4*c* site. However, as in the case of the antimonides $RE_5Tt_xSb_{3-x}$ [6], the possibility of disorder within these sites had to be considered. Depressed displacement parameters on the 4*c* site suggested partial mixing with Bi atoms. Refinement of this model led to occupancies of 87% Si and 13% Bi in this site. The resulting formula, $Ce_5Si_{0.869(4)}Bi_{2.131(4)}$, matches with the lower limit of the solid solution range, an understandable outcome given that the crystal was obtained under conditions that correspond to a deficiency of Si. Because of its proximity to the idealized composition, we refer to the formula Ce_5SiBi_2 for simplicity in subsequent discussion.

Powder X-ray diffaction data for Ce_5GeBi_2 were refined with the full-profile Rietveld method with use of the program LHPM-Rietica [20]. Initial positions were taken from the single-crystal structure above. The least-squares refinement included scale factor, background, zero point, cell parameters, pseudo-Voigt peak profile parameters, atomic coordinates, and isotropic displacement parameters. With the ordered model (Bi in 8*d* site and Ge in 4*c* site) being assumed, the fit of the Rietveld refinement results to the powder diffraction pattern is shown in Fig. 1. Instabilities encountered during the refinement of the displacement parameters were partly obviated by constraining their values to be equal for all four Ce atoms. The small value of U_{iso} found for the Bi1 site may be an artifact of these difficulties. The sample also contained a trace amount ($< 0.5\%$) of Ce_3Ge.

The cell parameters obtained from the single-crystal data are slightly different from those refined from powder data (Table 1), presumably because of minor variations in composition arising

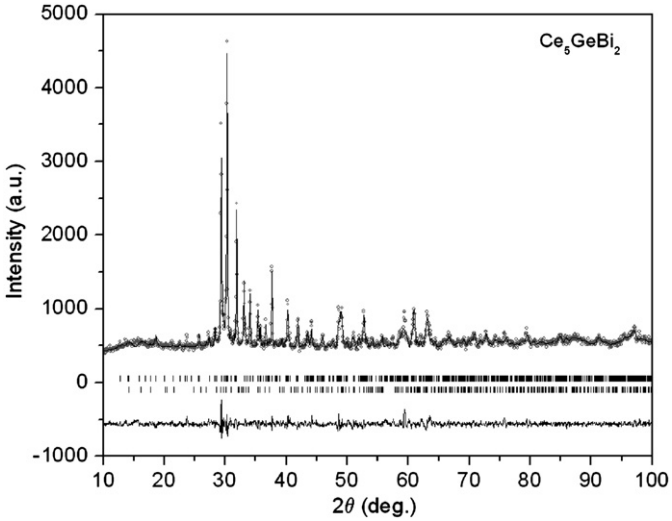

Fig. 1. Rietveld refinement results for Ce_5GeBi_2. The observed profile is indicated by circles and the calculated profile by the solid line. Bragg peak positions are located by the upper set of vertical tick marks; the lower set corresponds to trace amounts of Ce_3Ge. The difference plot is shown at the bottom.

from Bi volatilization, difficult to control during the arc-melting process. Atomic positions were standardized with the program STRUCTURE TIDY [21]. Crystal data and further details of the data collection are given in Table 2. Final values of the positional and displacement parameters are given in Table 3. A detailed listing of interatomic distances is given in Table S3 in Supplementary Data, and an abridged version is given in Table 4. Further data, in CIF format, have been sent to Fachinformationszentrum Karlsruhe, Abt. PROKA, 76344 Eggenstein-Leopoldshafen, Germany, as supplementary material No. CSD-422217 and can be obtained by contacting FIZ (quoting the article details and the corresponding CSD numbers).

2.3. Band structure calculations

Tight-binding linear muffin tin orbital (TB-LMTO) band structure calculations were performed on La_5SiBi_2 within the local density and atomic spheres approximation with use of the Stuttgart TB-LMTO program [22]. The basis sets consisted of La 6*s*/6*p*/5*d*/4*f*, Si 3*s*/3*p*/3*d*, and Bi 6*s*/6*p*/6*d*/5*f* orbitals, with the La 6*p*, Si 3*d*, and Bi 6*d*/5*f* orbitals being downfolded. Integrations in reciprocal space were carried out with an improved tetrahedron method over 100 irreducible *k* points.

2.4. X-ray photoelectron spectroscopy

XPS spectra for La_5GeBi_2 and Ce_5GeBi_2 were measured on a Kratos AXIS 165 spectrometer equipped with a monochromatic Al *K*α X-ray source (15 kV, 14 mA) and a hybrid lens with a spot size of 700 μm × 400 μm. The typical precision of this instrument is ± 0.1 eV. With all handling carried out within an Ar-filled glove box, the samples were ground into fine powder, pressed onto In foil, and mounted with adhesive carbon tape on a Cu sample holder. The samples were transferred within a sealed container to the analysis chamber of the XPS instrument. The pressure inside the analysis chamber was maintained at 10^{-7} to 10^{-9} Pa. The samples were sputter-cleaned with an Ar^+ ion beam (4 kV, 10 mA) to reduce the presence of surface oxides.

High-resolution core-line spectra were collected with an energy envelope of 80 eV (*RE* 3d peak) or 20 eV (Bi 4*f* and Ge 3*d* peaks), a pass energy of 20 eV, a step size of 0.05 eV, and a sweep time of 180 s. The spectra were calibrated against the C 1*s* line, arising from adventitious carbon, at 284.8 eV. The CasaXPS software package was used to analyze these spectra [23]. The background arising from energy loss was removed by applying a Shirley-type function and the peaks were fitted to pseudo-Voigt (70% Gaussian and 30% Lorentzian) line profiles. The Ge 3*d* spectra exhibited significant reduction after the Ar^+ sputtering procedure and were deemed to

Table 2
Crystallographic data for Ce_5SiBi_2 and Ce_5GeBi_2.

Formula	$Ce_5Si_{0.869(4)}Bi_{2.131(4)}$	Ce_5GeBi_2
Formula mass (amu)	1169.26	1191.15
Space group	*Pnma* (No. 62)	*Pnma* (No. 62)
a (Å)	12.6368(7)	12.6354(6)
b (Å)	9.5556(6)	9.5752(5)
c (Å)	8.3736(5)	8.3316(5)
V (Å^3)	1011.13(10)	1008.01(9)
Z	4	4
ρ_{calcd} (g cm^{-3})	7.681	7.849
Radiation	Mo *K*α, λ = 0.71073 Å	Cu *K*α, λ = 1.54051 Å
μ (mm^{-1})	58.88	240.19
2θ range	5.84–66.30°	10.00–100.00°
Refinement method	SHELXTL	Rietveld
No. of data collected	12449	3103 data points
No. of unique data	2005 (R_{int} = 0.064) (1749 with $F_o^2 > 2\sigma(F_o^2)$)	621 Bragg reflections
No. of variables	45	38
Residuals[a]	$R(F)$ ($F_o^2 > 2\sigma(F_o^2)$) = 0.044 $R_w(F_o^2)$ = 0.096	R_B = 0.025 R_p = 0.051 R_{wp} = 0.066

[a] $R(F) = \Sigma||F_o|-|F_c||/\Sigma|F_o|$; $R_w(F_o^2) = [\Sigma[w(F_o^2-F_c^2)^2]/\Sigma wF_o^4]^{1/2}$, $w^{-1} = [\sigma^2(F_o^2)+(Ap)^2+Bp]$ where $p = [\max(F_o^2,0)+2F_c^2]/3$; $R_B = \Sigma|I_o-I_c|/\Sigma I_o$; $R_p = \Sigma|y_o-y_c|/\Sigma y_o$; $R_{wp} = [\Sigma[w(y_o-y_c)]/\Sigma wy_o^2]^{1/2}$.

Table 4
Ranges of interatomic distances (Å) in Ce_5SiBi_2 and Ce_5GeBi_2.

	Ce_5SiBi_2	Ce_5GeBi_2
Ce1–*Tt*2	2.990(1)–3.166(2)	3.00(1)–3.30(1)
Ce1–Bi1	3.461(1)–3.600(1)	3.54(1)–3.60(1)
Ce2–*Tt*2	3.197(3)	3.17(1)
Ce2–Bi1	3.328(1)–3.332(1)	3.09(1)–3.53(1)
Ce3–*Tt*2	2.982(3)	3.31(1)
Ce3–Bi1	3.342(1)–3.366(1)	3.34(1)–3.35(1)
Ce4–*Tt*2	2.962(3)	2.91(1)
Ce4–Bi1	3.366(1)–3.405(1)	3.34(1)–3.41(1)
Bi1–Ce	3.328(1)–3.600(1)	3.09(1)–3.60(1)
*Tt*2–Ce	2.962(3)–3.197(3)	2.91(1)–3.31(1)
Shortest Ce–Ce	3.608(1)	3.51(1)

Table 3
Positional and equivalent isotropic displacement parameters for Ce_5SiBi_2 and Ce_5GeBi_2.

Atom	Wyckoff position	*x*	*y*	*z*	U_{eq} or U_{iso} (Å^2)[a]
Ce_5SiBi_2					
Ce1	8*d*	0.06276(5)	0.04309(7)	0.18712(7)	0.0164(2)
Ce2	4*c*	0.00194(6)	1/4	0.53723(11)	0.0137(2)
Ce3	4*c*	0.21290(8)	1/4	0.84145(11)	0.0175(2)
Ce4	4*c*	0.29514(7)	1/4	0.36950(11)	0.0147(2)
Bi1	8*d*	0.32576(3)	0.01094(4)	0.07786(5)	0.0119(1)
Si2/Bi2[b]	4*c*	0.4824(2)	1/4	0.5822(3)	0.0181(8)
Ce_5GeBi_2					
Ce1	8*d*	0.059(1)	0.053(1)	0.186(2)	0.022(2)
Ce2	4*c*	−0.022(1)	1/4	0.521(2)	0.022(2)
Ce3	4*c*	0.217(1)	1/4	0.829(2)	0.022(2)
Ce4	4*c*	0.294(1)	1/4	0.357(2)	0.022(2)
Bi1	8*d*	0.326(1)	0.010(2)	0.069(1)	0.002(2)
Ge2	4*c*	0.459(2)	1/4	0.600(2)	0.028(9)

[a] Values of U_{eq} (defined as one-third of the trace of the orthogonalized U_{ij} tensor) are listed for Ce_5SiBi_2 and values of U_{iso} are listed for Ce_5GeBi_2.
[b] Refined occupancies are 0.869(4) Si2 and 0.131(4) Bi2.

be unreliable. Only the *RE* 3*d* and Bi 4*f* spectra, which did not suffer from such reduction, will be presented.

2.5. Magnetic measurements

Measurements of dc magnetic susceptibility were made on powders of La_5GeBi_2, Ce_5SiBi_2, Ce_5GeBi_2, Pr_5SiBi_2, and Pr_5GeBi_2 between 2 and 300 K on a Quantum Design 9T–PPMS dc magnetometer/ac susceptometer. The susceptibility was corrected for contributions from the holder and underlying sample diamagnetism.

3. Results and discussion

3.1. Structure

The compounds RE_5TtBi_2 (*Tt*=Si, Ge) are a new series of ternary bismuthides that adopt the orthorhombic β-Yb_5Sb_3-type structure, different from that found for the binary bismuthides RE_5Bi_3 (Mn_5Si_3-type for the early *RE* and Y_5Bi_3-type for the late *RE*) [1]. In contrast to the previously known antimonides $RE_5Tt_xSb_{3-x}$, which occur only for *RE*=La–Nd and which exhibit a considerable phase width (e.g., $0.9 \le x \le 1.6$ for $La_5Ge_xSb_{3-x}$) [6], the bismuthides $RE_5Tt_xBi_{3-x}$

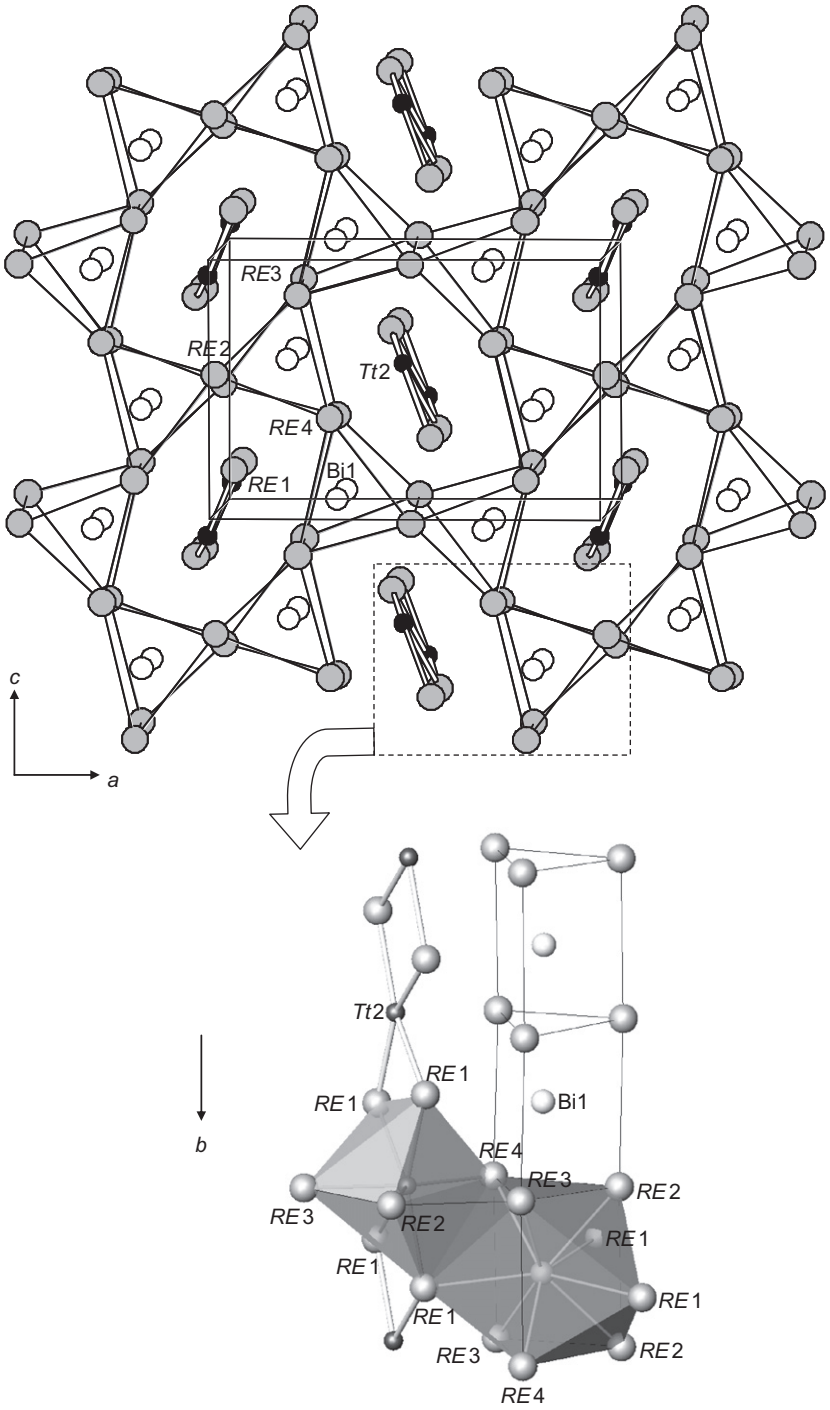

Fig. 2. Structure of RE_5TtBi_2 (*Tt*=Si, Ge) built up from Bi-centered RE_6 trigonal prisms and chains of $[RE_2Tt_2]$ rhombs, with the local coordination environments of *Tt*2 (4*c* site, CN7) and Bi1 (8*d* site, CN9) surrounded by *RE* atoms highlighted in the bottom panel.

occur with a more extensive range of *RE* substitution (*RE*=La–Nd, Gd–Er) but with a narrower phase width (e.g., $0.9 \le x < 1.0$ for $Ce_5Si_xBi_{3-x}$). For brevity, we assume the idealized formulation RE_5TtBi_2, which may also be characterized as a Ce_5RuGe_2-type (ordered β-Yb_5Sb_3-type) structure [24]. Note the absence of ternary RE_5TtBi_2 compounds for *RE*=Sm and presumably Eu, i.e. those *RE* metals that can be nominally divalent and which are also known to form interstitially stabilized hydrides RE_5Bi_3H (*RE*=Sm, Eu, Yb) with, interestingly, a stuffed β-Yb_5Sb_3-type structure [16,25].

The structure of RE_5TtBi_2 (*Tt*=Si, Ge) features Bi-centered edge-sharing RE_6 trigonal prisms defining large distorted hexagonal channels within which lie chains of corner-sharing rhombs made up of *RE* and *Tt* atoms (Fig. 2). Consistent with the coordination environments of *RE* atoms around the anions, the larger Bi atoms occupy the 8*d* site (CN9, tricapped trigonal prismatic) and the smaller *Tt* atoms occupy the 4*c* site (CN7, capped octahedral), although the existence of the narrow phase width implies that a limited mixing of these atoms is possible. The lesser tendency for these bismuthides, relative to the antimonides, to experience disorder between the pnicogen and *Tt* atoms may be attributed to the enhanced atomic size differences (cf. Pauling metallic radii R_1 of 1.17 Å for Si, 1.24 Å for Ge, 1.39 Å for Sb, and 1.51 Å for Bi) [26].

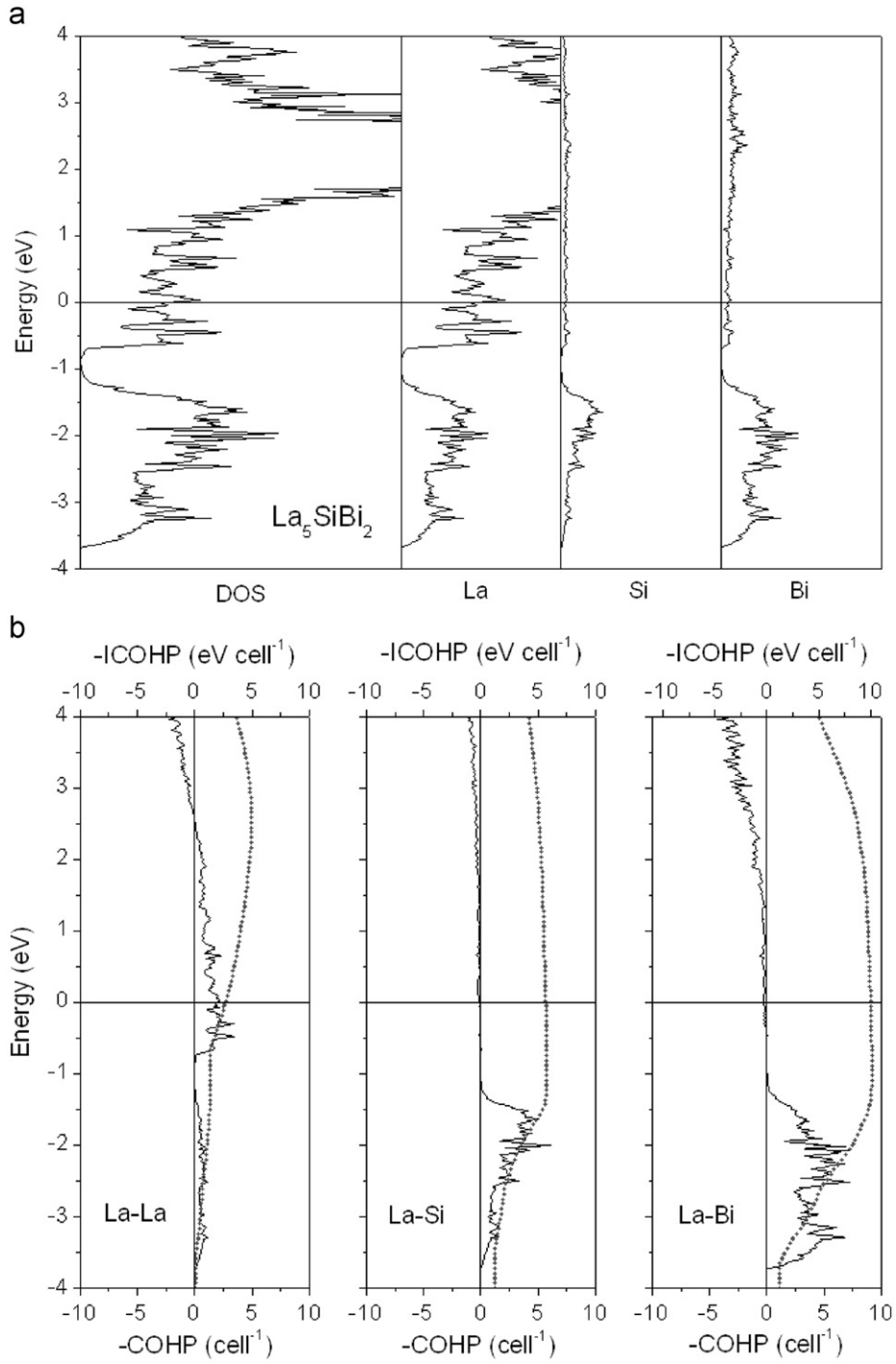

Fig. 3. (a) Density of states (DOS) and its La, Si, and Bi projections for La_5SiBi_2. (b) Crystal orbital Hamilton population (COHP) curves (solid line) and integrated COHP curves (dotted line) for La–La, La–Si, and La–Bi interactions. The horizontal lines at 0 eV mark the Fermi level.

For example, the demarcation of Bi–Ce (3.328(1)–3.600(1) Å) and Si–Ce (2.962(3)–3.197(3) Å) distances in $Ce_5Si_{0.9}Bi_{2.1}$ is more pronounced than the Sb–Ce (3.236(9)–3.539(5) Å) and Si–Ce (2.92(3)–3.27(2) Å) distances in $Ce_5Si_{1.4}Sb_{1.6}$ [6]. This explanation does not hold for Ce_5GeBi_2, where the distances are more irregular (Bi–Ce, 3.09(1)–3.60(1) Å; Ge–Ce, 2.91(1)–3.31(1) Å) suggesting a more distorted structure, although we note that this structure determination is less precise and no attempt was made to refine occupancies from the powder diffraction data here.

The greater extent of *RE* substitution in RE_5TtBi_2 (*RE*=La–Nd, Gd–Er) compared to RE_5TtSb_2 (*RE*=La–Nd) seems surprising at first glance, given the expectation that expansion of the bismuthide structures should be compatible with the larger *RE* atoms, not smaller ones. Previously we invoked arguments based on radius ratio rules to rationalize the preference of Sb atoms in the 8*d* site vs. *Tt* atoms in the 4*c* site in RE_5TtSb_2 [6]. Although it is true that the ratios r_{Sb}/r_{RE} (0.82 in La_5TtSb_2 to 0.85 in Nd_5TtSb_2) exceed the critical value of 0.73 required for the tricapped trigonal prismatic geometry of the pnicogen atom in the 8*d* site [27], they also appear to establish 0.85 as an upper limit. In the bismuthides RE_5TtBi_2, the ratios r_{Bi}/r_{RE} would range from 0.89 in La_5TtBi_2 to 0.95 in Er_5TtBi_2. This observation seems counterintuitive unless we appeal to the role of electron transfer. On the assumption that the pnicogen atoms accept electrons to become slightly anionic, both Sb and Bi atoms will have larger radii than the neutral species, but the size increase will be more pronounced for the more electronegative Sb atoms. That is, the values of r_{Sb}/r_{RE} would need to be corrected to yield a higher upper critical limit.

Alternatively, the contribution of *RE*–*RE* bonding, which has been suggested to be important in stabilizing this structure type relative to the binary phases [7,14], may be considered, as is evident from the surplus of valence electrons available on the *RE* atoms even after full transfer to the *Tt* and Bi atoms is assumed, i.e. $(RE^{3+})_5(Tt^{4-})(Bi^{3-})_2(e^-)_5$. For this purpose, a band structure calculation was conducted on La_5SiBi_2. Similar to previous calculations on La_5GeSb_2 [6], the density of states (DOS) curve reveals that most of the Si and Bi states are occupied below the Fermi level, mixing strongly with La states below −1 eV (Fig. 3a) to give rise to La–Si and La–Bi bonding interactions as seen in the crystal orbital Hamilton population (COHP) curves (Fig. 3b). These bonding interactions are optimized at −1 eV, at a lower electron count that would correspond to the nonexistent compound "Ba_5SiBi_2". Instead, because additional La–La bonding levels are available at higher energy, with the states near the Fermi level being nearly entirely La-based, a higher electron count can be supported. The average integrated COHP values (–ICOHP) for the La–Si (1.13 eV/bond) and La–Bi (0.67 eV/bond) interactions in La_5SiBi_2 are slightly larger or similar to the La–Ge (1.09 eV/bond) and La–Sb (0.68 eV/bond) interactions in La_5GeSb_2. However, as a result of the expanded bismuthide structure, the La–La interactions are slightly weaker in La_5SiBi_2 (0.22 eV/bond) than in La_5GeSb_2 (0.24 eV/bond). Extension of the

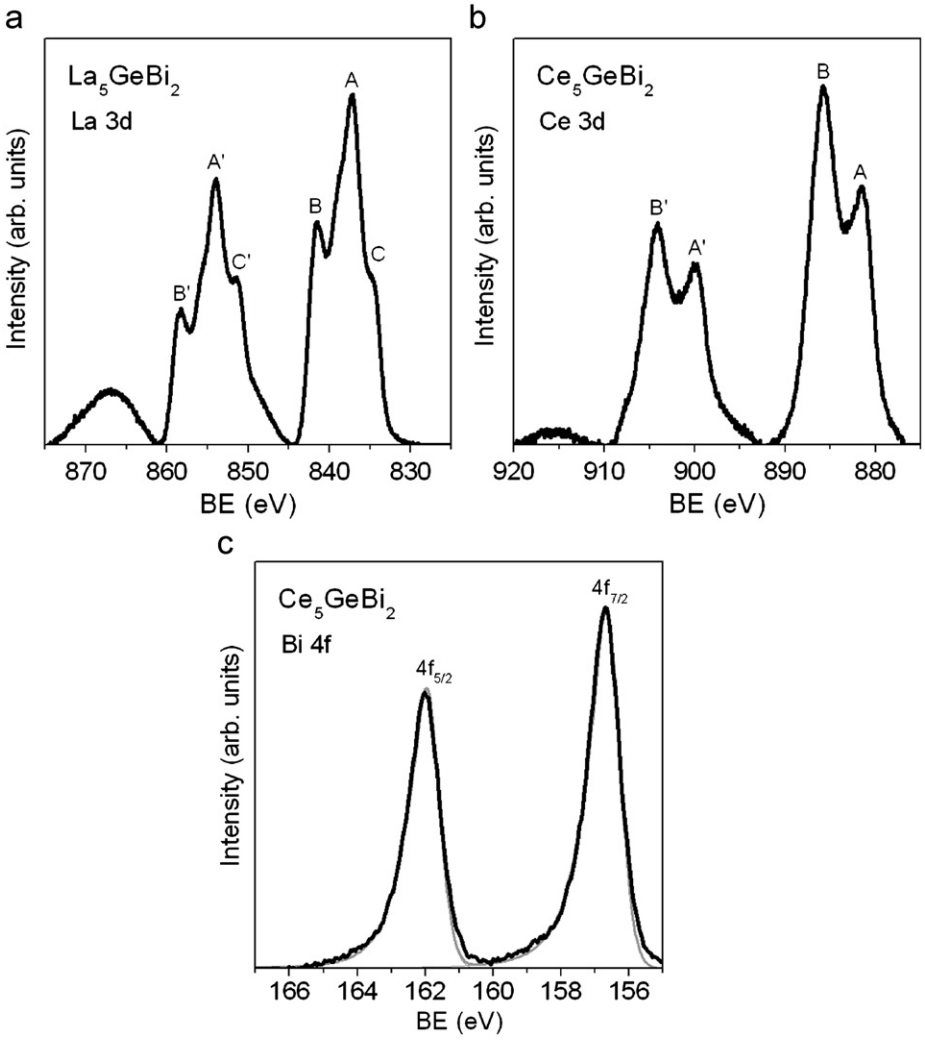

Fig. 4. (a) La 3*d*, (b) Ce 3*d*, and (c) Bi 4*f* XPS spectra for La_5GeBi_2 and Ce_5GeBi_2.

RE_5TtBi_2 series to smaller *RE* metals would then be able to counteract these diminished interactions.

3.2. XPS analysis

The *RE* 3*d* and Bi 4*f* XPS spectra for La_5GeBi_2 and Ce_5GeBi_2 were measured to provide experimental evidence for the electronic structure of these compounds. The La 3*d* and Ce 3*d* XPS spectra consist of two main core-line peaks representing the $3d_{5/2}$ (A) and $3d_{3/2}$ (A′) spin–orbit-coupled final states (Fig. 4a–b). The *RE* $3d_{5/2}$ binding energies (BEs) are 837.3 eV for La_5GeBi_2 and 881.7 eV for Ce_5GeBi_2, but they cannot be easily related to valence states because the 4f electrons poorly screen the nuclear charge, resulting in greater sensitivity to coordination environment and final state effects [28,29]. Instead, the more diagnostic feature is the lineshape, which is typical for the spectra of other trivalent La and Ce compounds such as $LaFe_4Sb_{12}$ and $CeFe_4Sb_{12}$ [30]. The occurrence of satellite peaks (B and B′) at higher BE to the respective core-line peaks can be attributed to a ligand-to-metal charge-transfer shake-up process, which is enhanced with greater orbital overlap between metal and ligand atoms [31,32]. Thus, the more intense satellites seen in the Ce spectra are consistent with the participation of *f* orbitals (arising from the $4f^1$ configuration of trivalent cerium) in bonding to the surrounding Ge and Bi atoms. Interestingly, a second set of satellite peaks (C and C′) is found at lower BE to the respective core-line peaks in La_5GeBi_2. This feature is also observed in the antimonides LaSb and $LaFe_4Sb_{12}$ (but not in the corresponding phosphides LaP and $LaFe_4P_{12}$) for which a two-core-hole process has been proposed [29,30,33]. As in these antimonides, strong covalent character may be assumed for bonds to the La atoms in La_5GeBi_2 with available La 4*f* states found near the Fermi level (as seen in the DOS curve for La_5SiBi_2 earlier). The core hole produced after photoionization pulls La 4*f* conduction states below the Fermi edge, creating a well-screened final state such that the photoelectron is ejected with higher kinetic energy, giving rise to a satellite peak with lower BE. The corresponding satellites are absent in Ce_5GeBi_2 presumably because the Ce 4*f* states are already entirely involved in bonding.

The Bi 4f XPS spectrum for Ce_5GeBi_2 consists of two peaks assigned as the $4f_{7/2}$ and $4f_{5/2}$ spin–orbit-coupled final states, in the expected intensity ratio of 4:3 (Fig. 4c). (The spectrum for La_5GeBi_2, not shown, is essentially identical in lineshapes and BEs.) The asymmetric lineshapes, skewed towards higher BE, are characteristic of metallic systems in which the core hole that remains after photoionization interacts with valence electrons, exciting them into the continuum of empty conduction states above the Fermi edge [34]. Electronic delocalization causes the core electrons to experience greater

Table 5
Summary of magnetic data for RE_5TtBi_2 (*RE*=Ce, Pr; *Tt*=Si, Ge).

	Ce_5SiBi_2	Ce_5GeBi_2	Pr_5SiBi_2	Pr_5GeBi_2
T_N (K)	3	<2	8	8, 33
θ_p (K)	9.2(3)	4.3(1)	27.3(5)	37.7(6)
$\mu_{eff,\ meas}$ (μ_B/*RE*)	2.59(1)	2.51(1)	3.91(3)	3.50(4)
$\mu_{eff,\ theor}$ for RE^{3+} (μ_B)	2.54	2.54	3.58	3.58
χ_o (emu mol^{-1})	0.00238(1)	0.0081(1)	0.0186(3)	0.0071(3)

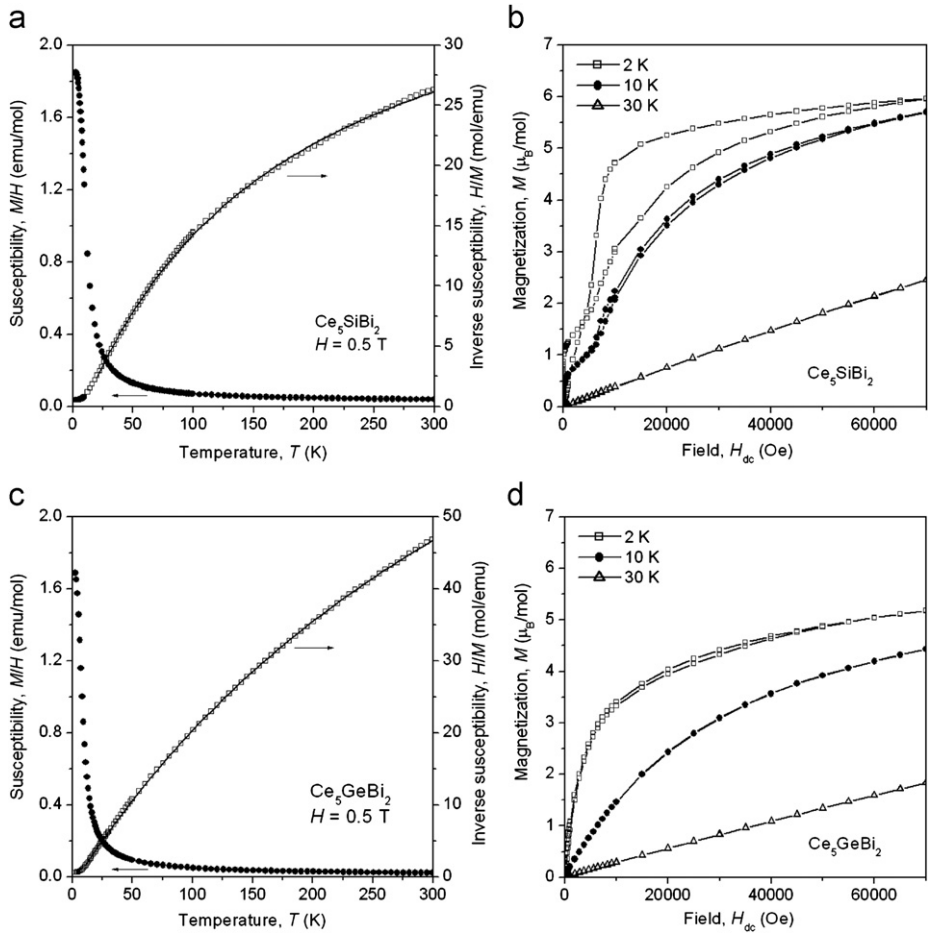

Fig. 5. Magnetic data for (a)–(b) Ce_5SiBi_2 and (c)–(d) Ce_5GeBi_2. The left panels show the zero-field-cooled dc magnetic susceptibility and its inverse; the right panels show magnetization curves at different temperatures.

nuclear screening, such that the $4f_{7/2}$ BE in Ce_5GeBi_2 (156.7 eV) is close to that in elemental Bi (157.0(1) eV) [35]. The small negative shift in BE, which is also similar to that observed in $LaGaBi_2$ (156.6 eV) [2], supports the presence of anionic Bi atoms in Ce_5GeBi_2.

3.3. Magnetic properties

The presence of a large number of *RE* atoms in proximity (e.g. >3.5 Å in Ce_5SiBi_2 and Ce_5GeBi_2) gives rise to potential magnetic interactions in the RE_5TtBi_2 series. Although La_5GeBi_2 exhibits only temperature-independent paramagnetism with $\chi_o=0.007$ emu/mol (Fig. S3 in Supplementary Data), the Ce and Pr members are more interesting, as summarized in Table 5.

The magnetic susceptibility of Ce_5SiBi_2 undergoes a slight downturn as the temperature decreases below 3 K (Fig. 5a), near the limits of our instrumentation. At higher temperature, the inverse magnetic susceptibility curve shows a marked curvature. Fitting in this paramagnetic regime to the modified Curie–Weiss law, $\chi=C/(T-\theta_p)+\chi_o$, yielded an effective magnetic moment (derived from the Curie constant *C*) of 2.59 μ_B/Ce, close to the theoretical free-ion value of 2.54 μ_B for trivalent cerium and consistent with the XPS data. However, the positive Weiss parameter θ_p of 9.2 K implies ferromagnetic coupling between the Ce ions. Accordingly, at 2 K, just below the transition temperature, the isothermal magnetization curve exhibits hysteresis and an approach to saturation, along with at least two field-dependent transitions (Fig. 5b). Even at 10 K, these transitions are still visible. A possible interpretation of these observations is a ferrimagnetic structure undergoing spin reorientation at different fields. The behavior of Ce_5GeBi_2 is similar but with much less pronounced curvature in the inverse magnetic susceptibility (Fig. 5c) and the disappearance of the field-dependent transitions (Fig. 5d). Although the tetrel atoms lack localized unpaired electrons, it is clear that they can influence the magnetic behavior.

The temperature dependence of the magnetic susceptibility of Pr_5SiBi_2 (Fig. 6a) appears similar to that of Ce_5SiBi_2, with the downturn occurring at a higher temperature of 8 K. Fitting of the inverse magnetic susceptibility to the modified Curie–Weiss law gave an effective magnetic moment of 3.91 μ_B/Pr. This is somewhat higher than the theoretical value of 3.58 μ_B for Pr^{3+}, perhaps because of polarization of conduction electrons, the important contribution of which is indicated by the large value of χ_o derived from the Curie–Weiss fit. Hysteresis and saturation are evident in the magnetization curve at 2 K (Fig. 6b). The downturn at 8 K is retained in Pr_5GeBi_2, but a second transition emerges at 33 K (Fig. 6c). The magnetization curve at 10 K, between these two temperatures, reveals distinctly different field-dependent transitions than at 2 K (Fig. 6d). The behavior of Pr_5SiBi_2 and Pr_5GeBi_2 parallels that of the antimonides, $Pr_5Si_{1.2}Sb_{1.8}$ and $Pr_5Ge_{1.2}Sb_{1.8}$, examined previously, which have similar magnetic susceptibility and magnetization curves [6]. These similarities reinforce the point made above that the tetrel atoms play a more important role than the pnicogen atoms in modifying the interactions between the *RE* atoms.

4. Conclusions

Although the β-Yb_5Sb_3-type structure is adopted by none of the binary bismuthides RE_5Bi_3, it can be formed through replacement

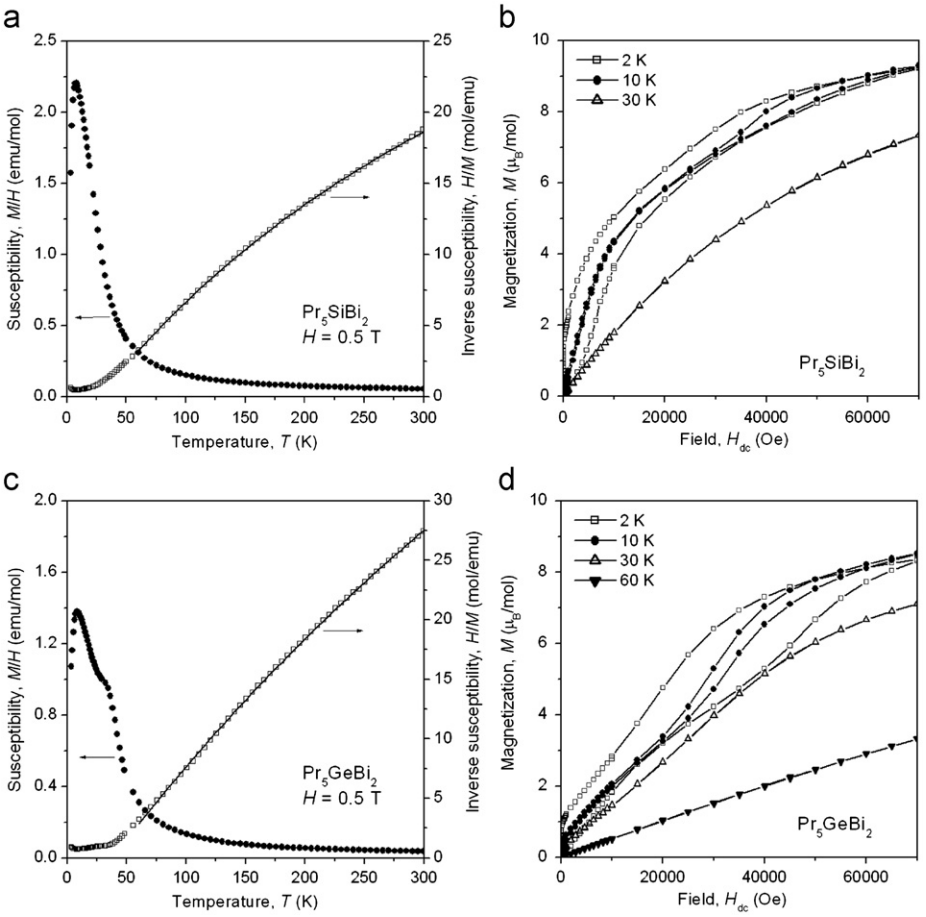

Fig. 6. Magnetic data for (a)–(b) Pr_5SiBi_2 and (c)–(d) Pr_5GeBi_2. The left panels show the zero-field-cooled dc magnetic susceptibility and its inverse; the right panels show magnetization curves at different temperatures.

of Bi with a tetrel atom (Si or Ge) in the ternary bismuthides RE_5TtBi_2. (An interesting example of the antitype structure is provided by U_3S_5, containing both tetravalent and trivalent uranium atoms, as represented by the formulation $(U^{3+})_2(U^{4+})(S^{2-})_5$ [36,37].) This series is surprisingly more extensive in terms of *RE* substitution, extending from La to Er, than the counterparts with antimonides, RE_5TtSb_2 (*RE*=La–Nd) or with transition metals, RE_5MBi_2 (*RE*=Gd–Er). Although partial mixing of *Tt* and Bi atoms still occurs, the enhanced size difference reduces the phase width drastically so that the structure becomes essentially ordered. XPS analysis supports the presence of trivalent *RE* and slightly anionic Bi atoms in these compounds. The magnetic properties originate from interactions between f electrons between the *RE* atoms but they are strongly influenced by the nature of the *Tt* atoms.

Acknowledgments

The Natural Sciences and Engineering Research Council of Canada and the Donors of the American Chemical Society Petroleum Research Fund are acknowledged for support of this research. We thank Dr. Robert McDonald and Dr. Michael J. Ferguson (X-ray Crystallography Laboratory) for assistance with the single-crystal X-ray data collection, and Ms. Christina Barker (Department of Chemical and Materials Engineering) and Ms. De-Ann Rollings (Department of Earth and Atmospheric Sciences) for the EDX analyses. Access to the Kratos AXIS 165 XPS spectrometer was provided by the Alberta Centre for Surface Engineering and Science, which was established with support from the Canada Foundation for Innovation and Alberta Innovation and Science.

Appendix A. Supplementary materials

Supplementary data associated with this article can be found in the online version at doi:10.1016/j.jssc.2010.10.007.

References

[1] A. Mar, in: K.A. Gschneidner Jr., J.-C.G. Bünzli, V.K. Pecharsky (Eds.), Handbook on the Physics and Chemistry of Rare Earths, vol. 36, Elsevier, Amsterdam, 2006, pp. 1–82.
[2] M.G. Morgan, M. Wang, W.Y. Chan, A. Mar, Inorg. Chem. 42 (2003) 1549–1555.
[3] J.Y. Chan, M.E. Wang, A. Rehr, S.M. Kauzlarich, D.J. Webb, Chem. Mater. 9 (1997) 2131–2138.
[4] A.O. Stetskiv, V.V. Pavyluk, O.I. Bodak, Ukr. Khim. Zh. 64 (1998) 22–24.
[5] V. Svitlyk, B.J. Campbell, Y. Mozharivskyj, Inorg. Chem. 48 (2009) 10364–10370.
[6] H. Bie, A. Mar, Eur. J. Inorg. Chem. (2009) 3403–3413.
[7] Y. Mozharivskyj, H.F. Franzen, J. Alloys Compd. 319 (2001) 100–107.
[8] A.V. Morozkin, R. Nirmala, S.K. Malik, J. Alloys Compd. 394 (2005) L5–L9.
[9] M. Zelinska, O. Zhak, S. Oryshchyn, V. Babizhetskyy, J.-Y. Pivan, R. Guérin, J. Alloys Compd. 437 (2007) 133–139.
[10] Yu. Verbovytsky, K. Łątka, J. Alloys Compd. 450 (2008) 272–275.
[11] V. Svitlyk, F. Fei, Y. Mozharivskyj, J. Solid State Chem. 181 (2008) 1080–1086.
[12] V. Svitlyk, F. Fei, Y. Mozharivskyj, Solid State Sci. 11 (2009) 1700–1702.
[13] G.D. Brunton, H. Steinfink, Inorg. Chem. 10 (1971) 2301–2303.
[14] S. Gupta, E.A. León-Escamilla, F. Wang, G.J. Miller, J.D. Corbett, Inorg. Chem. 48 (2009) 4362–4371.
[15] Y. Liang, R. Cardoso-Gil, W. Schnelle, M. Schmidt, J.T. Zhao, Y. Grin, Z. Naturforsch. B: J. Chem. Sci. 62 (2007) 935–940.
[16] E.A. Leon-Escamilla, P. Dervenagas, C. Stassis, J.D. Corbett, J. Solid State Chem. 183 (2010) 114–119.
[17] O. Ya. Zelinska, A. Mar, J. Alloys Compd. 451 (2008) 606–609.
[18] A.V. Tkachuk, T. Tam, A. Mar, Chem. Met. Alloys 1 (2008) 76–83.
[19] G.M. Sheldrick, SHELXTL, version 6.12, Bruker AXS Inc., Madison, WI, 2001.
[20] B. Hunter, LHPM-Rietica, version 1.7.7, International Union of Crystallography Commission on Powder Diffraction Newsletter, no. 20 (summer), 1998, ⟨http://www.rietica.org⟩.
[21] L.M. Gelato, E. Parthé, J. Appl. Crystallogr. 20 (1987) 139–143.
[22] R. Tank, O. Jepsen, A. Burkhardt, O.K. Andersen, TB-LMTO-ASA Program, version 4.7, Max Planck Institut für Festkörperforschung, Stuttgart, Germany, 1998.
[23] N. Fairley, CasaXPS, version 2.3.9, Casa Software Ltd., Teighnmouth, Devon, UK, 2003, ⟨http://www.casaxps.com⟩.
[24] R.E. Gladyshevskii, K. Cenzual, J.T. Zhao, E. Parthé, Acta Crystallogr., Sect. C: Cryst. Struct. Commun. 48 (1992) 221–225.
[25] E.A. Leon-Escamilla, J.D. Corbett, J. Alloys Compd. 265 (1998) 104–114.
[26] L. Pauling, The Nature of the Chemical Bond, 3rd ed., Cornell University Press, Ithaca, NY, 1960.
[27] A.F. Holleman, E. Wiberg, Inorganic Chemistry, Academic Press, San Diego, CA, 2001.
[28] W. Grünert, U. Sauerlandt, R. Schlögl, H.G. Karge, J. Phys. Chem. 97 (1993) 1413–1419.
[29] A.P. Grosvenor, R.G. Cavell, A. Mar, Chem. Mater. 18 (2006) 1650–1657.
[30] A.P. Grosvenor, R.G. Cavell, A. Mar, Phys. Rev. B 74 (2006) 125102-1–125102-10.
[31] T. Ikeda, K. Okada, H. Ogasawara, A. Kotani, J. Phys. Soc. Jpn. 59 (1990) 622–630.
[32] C.J. Niu, Y.Q. Jia, Spectrochim. Acta, Part A 49 (1993) 947–951.
[33] Y. Baer, R. Hauger, C. Zürcher, M. Campagna, G.K. Wertheim, Phys. Rev. B 18 (1978) 4433–4439.
[34] S. Doniach, M. Šunjić, J. Phys. C: Solid State Phys. 3 (1970) 285–291.
[35] C.D. Wagner, A.V. Naumkin, A. Kraut-Vass, J.W. Allison, C.J. Powell, J.R. Rumble Jr., NIST X-ray Photoelectron Spectroscopy Database, version 3.5 (web version), National Institute of Standards and Technology, Gaithersburg, MD, 2003, ⟨http://srdata.nist.gov/xps⟩.
[36] M. Potel, R. Brochu, J. Padiou, D. Grandjean, C. R. Seances Acad. Sci., Ser. C 275 (1972) 1419–1421.
[37] H. Kohlmann, H.P. Beck, J. Solid State Chem. 150 (2000) 336–341.